A New Nano-($2Li_2O/MgO$) Catalyst/Porous Alpha-Alumina Composite for the Oxidative Coupling of Methane Reaction

Behrooz Fallah
Ceramics Dept., Materials and Energy Research Center, Tehran, Iran

Cavus Falamaki
Ceramics Dept., Materials and Energy Research Center, Tehran, Iran

Chemical Engineering Dept., Amirkabir University of Technology, Tehran, Iran

DOI 10.1002/aic.12018
Published online August 20, 2009 in Wiley InterScience (www.interscience.wiley.com).

The present work discloses a new methodology for the production of detached nanorods of $2Li_2O/MgO$ catalyst particles on the internal surface of α-Al_2O_3 porous supports to be used as efficient catalysts for the oxidative coupling of methane reaction (OCM). The peculiarity of our preparatory recipe is the success in producing "detached" nanosized entities on the support surface. The performance of the new catalyst/support system for the OCM reaction has been evaluated using a special reactor assembly with cross flow of methane and oxygen gas streams. Under the optimum process conditions, the yield of C_2^+ product is 25% at an average reaction temperature of 750°C. Under the optimum conditions, the yield of ethylene reaches 8%. It is shown that the enhanced catalytic properties of the new catalyst/support composite may be attributed to nanoeffects. © 2009 American Institute of Chemical Engineers *AIChE J,* 56: 717–728, 2010

Keywords: nanocatalyst, nanoemulsion, Li_2O/MgO, α-Al_2O_3, oxidative coupling of methane

Introduction

Discovery of novel methods for the production of nanostructured $2Li_2O/MgO$ catalyst particles on the internal surface of porous carriers like α-Al_2O_3 is of extreme importance in catalyst engineering. For example, lithium-doped MgO is an effective catalyst for the oxidative coupling of methane (OCM).[1] On the other hand, such catalyst particles should be located on the external surface of nonporous or internal surface of porous carriers. The latter is of most importance, as the OCM reaction using porous ceramic membrane catalytic reactors has opened a new horizon in this area.[2,3]

Correspondence concerning this article should be addressed to C. Falamaki at c.falamaki@aut.ac.ir

Use of nanoemulsions for the synthesis of nano-oxide particles is a new and prosperous realm in nanocatalyst engineering. Surfactant-stabilized water-in-oil (W/O) emulsions have been successfully used as nanoreactors for the synthesis of Fe_3O_4,[4] TiO_2,[5,6] SiO_2[5] nanoparticles. The interesting work of Elm Svensson et al.[7] for the manufacture of nanocatalyst materials for high-temperature catalytic combustion of methane ($LaMnO_3$ supported on MgO) uses the reaction of two different microemulsion droplets containing the reacting species or the reaction of a diffusing component from the matrix phase to the nanodroplet.

This work discloses a new methodology for the production of detached nanorods of $2Li_2O/MgO$ catalyst particles on the internal surface of α-Al_2O_3 porous supports. We have adopted a nanoemulsion preparation technique (W/O system) for producing aqueous entrapped metal ion nanodroplets.

The method employed in this study for the production of nano-$2Li_2O$/MgO particles, using W/O nanoemulsions, follows a distinct, different philosophy compared with the preparatory recipes reported so far: (a) The droplets in the nanoemulsion are not used as nanoreactors during the synthesis step, (b) the nanodroplets are separated from the W/O system by infiltration of the latter into a porous media with subsequent wetting of the internal surface of the porous media with the nanoemulsion, and (c) the nanorods are finally obtained by proper heat treatment at high-temperature of the internally coated porous support.

A thorough study on the preparation of W/O nanoemulsions using nonionic surfactants has been reported recently by Porras et al.[8] Although such investigations are valuable, it will be shown that they cannot be directly used for the entrapment of water droplets containing ions as the nanoemulsion droplet size distribution will be different under similar operational conditions.

The first part of the article explains a simple methodology used for optimizing the amount of surfactant. The nanoemulsion droplet size distribution of the W/O system obtained by employing sole mechanical treatment at different mixing intensities and mechanical mixing, followed by ultrasound (US) treatment for different periods of time will be discussed. After selection of the best nanoemulsion preparatory method, the heat treatment procedure for obtaining detached nanoentities of the mixed oxides $2Li_2O$/MgO on the internal surface of α-Al_2O_3 porous supports will be investigated.

The preparation methods reported in open literature generally do allude to the sole production of "nanosized" catalyst particles (e.g., CeO_2/ZnO catalyst for the OCM reaction[9]). Nanoparticles by themselves are not attractive for industrial applications and should exist on carriers which provide mechanical strength, among other characteristics. This work considers the synthesis procedure of a nanocatalyst supported on the internal surface of an alpha-alumina porous support. The production of nanosized oxide catalyst particles has been reported in the past[9] with a low yield of C_2^+ products (<10 %) in the temperature range of 873–1098 K. To the knowledge of the authors of this work, the production of nanocatalyst/support complex structures has been the subject of just a few reports,[10,11] and no report on the specific OCM reaction system exists. It is noteworthy that forming nanostructures on support surfaces is a tricky task in materials engineering. Finding the optimum procedure for obtaining such a material is the main subject of the first part of this work.

The second part of the article studies the catalytic behavior of the manufactured nanocatalyst/support system for the OCM reaction. This system actually uses some sort of a "catalytic membrane" in the form of a cylindrical nanocatalyst/porous support body through which the reactants flow. In addition, a special reactor configuration has been implemented where the CH_4/Ar and O_2/Ar gas stream mixtures enter the system in a cross flow fashion in order to gradually introducing O_2 to the reacting mixture. It is well known that higher selectivity's of C_2^+ compounds are obtainable by distributing the O_2 supply to the reactor.[12] The effect of operating conditions (average reaction temperature, flow rates, inert gas concentration) at a constant CH_4/O_2 molar ratio equal to 1.6 has been investigated. The new catalyst shows promising results, as will be discussed in detail in what follows.

Experimental

Lithium nitrate hexahydrate (98.5 wt % purity) and hexahydrate magnesium nitrate (99.0 wt % purity) were purchased from MERCK. Commercial Iranian kerosene was used as the organic medium, and deionized water was used (Elga De-ionizer). A nonionic surfactant, SPAN 83, with an HLB value (hydrophilic-lipophilic balance) between four and six was used, and normal propanol was used as cosurfactant (Fluka).

The microemulsion synthesis procedure is as follows: Solution A is prepared by the addition of different volumes of a 50 wt % aqueous solution of SPAN 83 to 150 cm^3 kerosene under stirring. Around 1 cm^3 propanol (cosurfactant) is added to 3 cm^3 of an aqueous solution of lithium and magnesium nitrate salts (4 molar and 1 molar for lithium and magnesium, respectively) to obtain solution B. The latter is added dropwise to solution A and vigorously agitated using a propeller mixer for 25 min to obtain mixture C. Mixture C is subjected to severe agitation (550–1500 rpm) or ultrasound treatment (35 KHz frequency, 240 W power) for different time periods with or without prior vigorous agitation to obtain the final microemulsion D.

For the production of the catalyst/support composite, the following procedure was followed: Porous α-Al_2O_3 ceramic cylinders (diameter = 20 mm, height = 60 mm, sintered fused alpha alumina) with a porosity ca. 33% and average pore size ca. 100 μm were obtained from the Materials and Energy Research Center (MERC), Tehran, Iran. These were used as catalyst supports; the latter were infiltrated with mixture D for 20 min. The wet supports were then subjected to mild evaporation at 70°C for 1.5 h and afterward thermally treated at different temperatures (250–1250°C) for 1.5 h. The supports have high nitrogen gas permeability for gas flow through them due to their large pores (larger than 900 $cm^3\ min^{-1}\ bar^{-1}$). The catalytic tests were performed on the composite prepared with the following specific recipe: In the preparation of solution A, 2 cm^3 50 wt % SPAN 83 was used; microemulsion D was subjected to 25 min-ultrasound treatment; the calcination temperature of the dried infiltrated support has been 900°C.

"Conventional catalyst/support composites" were produced by simply impregnating the porous supports with an aqueous solution of lithium and magnesium nitrate salts (4 molar and 1 molar for lithium and magnesium, respectively) for 20 min. Further treatments follow the same procedure as aforementioned. This was performed for obtaining micron-sized catalyst particles on the support as a routine catalyst synthesis procedure.

Measurement of the droplets size distribution in mixture C was performed by the dynamic laser light scattering method with a Malvern instrument (Zetasizer 5000) using a helium-neon laser with a wave-length of 633 nm. Scanning electron microscopy (SEM) was performed using a Stereo Scan 360-Leica (Cambridge Instruments) apparatus. For the latter experiments, the treated porous support was cut and one of the "new" surfaces created were subjected to SEM analysis. Conductivity measurements were performed using an

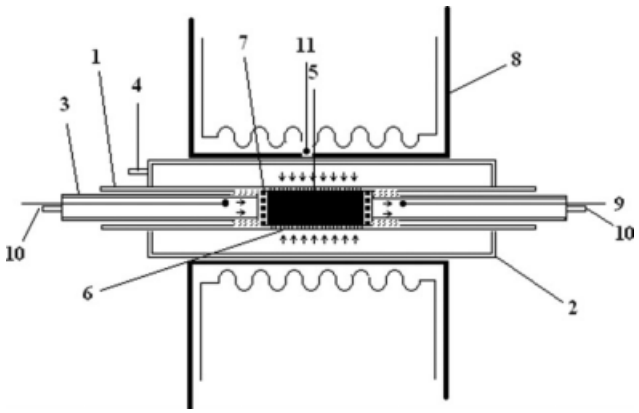

Figure 1. Reactor system configuration: (1) tube; (2) shell; (3) inner fixing tube; (4) shell gas stream inlet; (5) catalytic sintered membrane; (6) perforated tube side in contact with membrane; (7) perforated disk; (9) thermocouple; (10) tube gas stream inlet; (11) thermocouple.

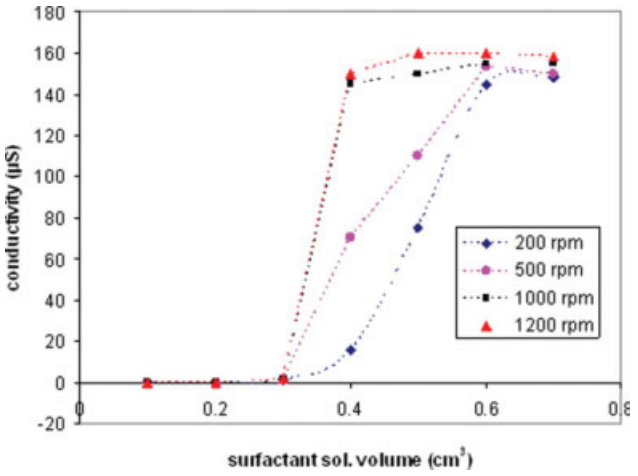

Figure 2. Conductivity as a function of surfactant concentration and mixing intensity.

[Color figure can be viewed in the online issue, which is available at www.interscience.wiley.com.]

ORION instrument (Research Conductivity Meter 101) with platinum electrodes at room temperature at different levels of agitation.

Simultaneous thermal analysis (STA) was performed using a Mettler DSC 821 (Mettler Toledo, D-Giesen) apparatus using a heating rate of 15°C min^{-1} with a nitrogen carrier gas flow rate of 80 cm^3 min^{-1}. Specific surface area measurements were done using nitrogen gas adsorption and applying the BET method. For this means, a Micromeritics Gemini 2375 apparatus (Norcross, GA) was used.

Chemical analysis of the Li and Mg content of the catalyst/support composite (nanocatalyst/support and conventional composite) was performed using the ICP technique (ICP-AES ARL-3410).

The reactor system configuration is shown in Figure 1. It consists mainly of a shell and tube configuration, and the sintered catalytic membrane is placed in the middle of the tube. Generally, CH_4 diluted with Ar passes through the tube side, whereas diluted O_2 passes through the shell side. The peripheral area of the tube in contact with the membrane is perforated with a large number of pores with a diameter of 1 mm. This allows diluted O_2 from the shell side to enter the membrane in a cross-flow fashion with respect to the axial flow of diluted CH_4. The entire shell and tube assembly is placed in an electrical furnace for temperature control. As shown in Figure 1, two thermocouples do indicate the inlet and outlet gas temperatures in the tube side. Temperature control is performed using a PID system having its feedback temperature at the outer shell side just at the middle of the shell and tube assembly (element 11 in Figure 1).

The shell side material was an Inconel alloy and the tube side material was 310 stainless steel. A special sealing system is used for fixing the rod-like membrane in the tube side. An inner fixing tube within the tube side fixes the membrane through threads in its ends (the inner wall of the tube has threads in the corresponding location) and imparting mechanical pressure on a perforated thick disk (element 7) in contact with the ceramic membrane.

The outlet form the reactor system passes through a water cooled condenser, enters a caustic solution for CO_2 removal, a drying unit for water exclusion and finally samples of the resulting stream are injected to a GC system (Perkin–Elmer Sigma 3B) with a TCD detector. A Propak Q column was used (100–200 mesh, 1.8 m length).

All kinetic experiments have been run at near atmospheric pressure. The maximum temperature difference between the outlet and inlet gas temperatures has been 30°C for an average reaction temperature of 750°C. The maximum temperature difference between the outer shell and the center of the reactor system has been measured to be 10°C.

Results and Discussion

Development of the nanocatalyst preparation method

The first step of the present investigation discloses a simple method employed for the determination of the minimum amount of surfactant needed for the production of the nanoemulsion based on conductivity measurement. It should be recalled that conduction titration is a classical technique for the manifestation of micelle formation[13] and is usually used

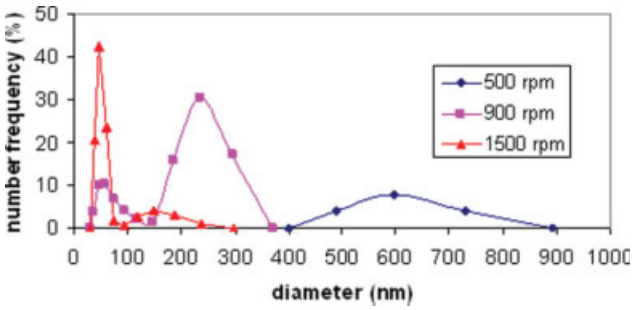

Figure 3. Droplets size distribution as a function of mixing intensity.

[Color figure can be viewed in the online issue, which is available at www.interscience.wiley.com.]

Table 1. Size Distribution Analysis Due to Different Treatments

Mixing Rate (rpm)	US	Time (min)	Avg. Diameter (nm) 1st Peak	Area (%) 1st Peak	Avg. Diameter (nm) 2nd Peak	Area (%) 2nd Peak
500	No	25	603	100	–	0
900	No	25	96	38	405	62
1500	No	25	49	89	157	11
500*	No	25	64	100	–	0
1000*	No	25	55	100	–	0
1500*	No	25	42	100	–	0
–	Yes	5	98	93	2857	7
–	Yes	25	42	100	–	0

*No ions present in the water phase.

for investigation of the O/W to W/O transitional zone in the phase inversion temperature method (PIT).[14]

For this means, the surfactant was added to mixture C after the vigorous agitation step was commenced and the conductivity was measured after 5 min. The results are shown in Figure 2. It is generally observed that an S-shaped curve results. Considering the agitation rate of 1200 rpm as a typical example, it is observed that at low surfactant concentrations, conductivity is negligible. As the surfactant concentration is increased, a sharp increase in the amount of conductivity is observed in a limited concentration region (between 0.3 and 0.4 cm^3 surfactant solution volume added). The conductivity ultimately reaches an asymptote.

Considering Figure 2, the following deductions can be made: (a) Increasing the agitation rate increases conductivity at constant surfactant concentration for surfactant solution added volume less than 0.6 cm^3, (b) the value of the conductivity asymptote increases with the increase of agitation rate and (c) the asymptote conductivity value is reached at smaller surfactant concentrations as the mixing rate is increased.

The explanation to the observed behavior is quite simple. At constant mixing rate, at low surfactant concentrations the size of the droplets is quite large due to lack of sufficient surfactant molecules for the stabilization of smaller droplets in the mixtures. With addition of sufficient surfactant at constant mixing rate, all small droplets produced because of the mixing power applied survive due to the dispersing effect imparted by the sufficient surfactant molecules around them. Stabilization of the small droplets increases the number of smaller charge carriers, thus increasing significantly the total conductivity. Addition of more surfactant has no effect on conductivity due to the limit imposed by the shear forces applied on the minimum size of droplets obtainable. On the other hand, as the agitation rate is increased, the average size of the droplets decreases resulting in smaller charge carriers and hence an increase in conductivity. The main outcome of the explained experiments is the presentation of a simple analytical tool for obtaining the optimum surfactant concentration needed for stabilizing the droplets with the size imparted by the shear rate power imposed. According to Figure 2, a surfactant solution addition of 0.6 cm^3 will be satisfactory for agitation rates larger than 500 rpm. Therefore, the latter value was chosen as the surfactant concentration for the droplets size distribution analysis experiments.

Figure 3 shows the droplets size distribution obtained employing 500, 900, and 1500 rpm agitation rates (in the presence of salts). Table 1 summarizes the peak analysis by number for the aforementioned experiments. At an agitation rate of 500 rpm, a broad peak with a volume average of 603 nm is observed. Increasing the agitation rate to 900 rpm, the curve detaches into two distinct peaks along a clear shift toward smaller sizes. Nonetheless, none of the peaks lies in the 1–100 nm size range. Increasing the mixing rate up to 1500 rpm, results in a more distinct peak detachment. Also, a clear peaks shift toward smaller sizes is observed. At this agitation rate, the main peak (89 area %) has an average value of 50 nm. It is therefore interesting that dominating nanosize droplets could be obtained by simple low-energy mechanical mixing.

At this stage, it would be interesting to show the effect of the presence of Li and Mg salts in the water solution A on the minimum size of droplets attainable. Figure 4 shows the droplets size distribution of the mixture C at a mixing rate of 500, 1000, and 1500 rpm in the absence of the foregoing salts (see Table 1 for statistical data). Interestingly, for the entire mixing rate employed, a mono-modal curve is observed. In addition, the average size decreases from 64 to 42 nm from 500 to 1500 rpm.

Clearly, it may be deduced that the addition of ionizable salts to water acts as an inhibiting factor to the production of smaller droplets. This can be explained resorting to the scheme shown in Figure 5. Only Li^+ and nitrate cations have been shown for sake of simplicity. The electric field of the Li^+ cations and nitrate anions tear water dipoles out of the water random lattice and eventually a "certain" number of water molecules get "immobilized" around them. This is a manifestation of the classical "solvation" phenomenon.[15] Therefore, the minimal attainable nanoemulsion droplet size

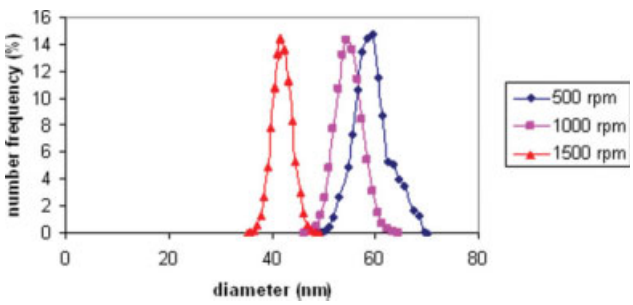

Figure 4. Droplets size distribution as a function of mixing intensity in the absence of Li and Mg salts.

[Color figure can be viewed in the online issue, which is available at www.interscience.wiley.com.]

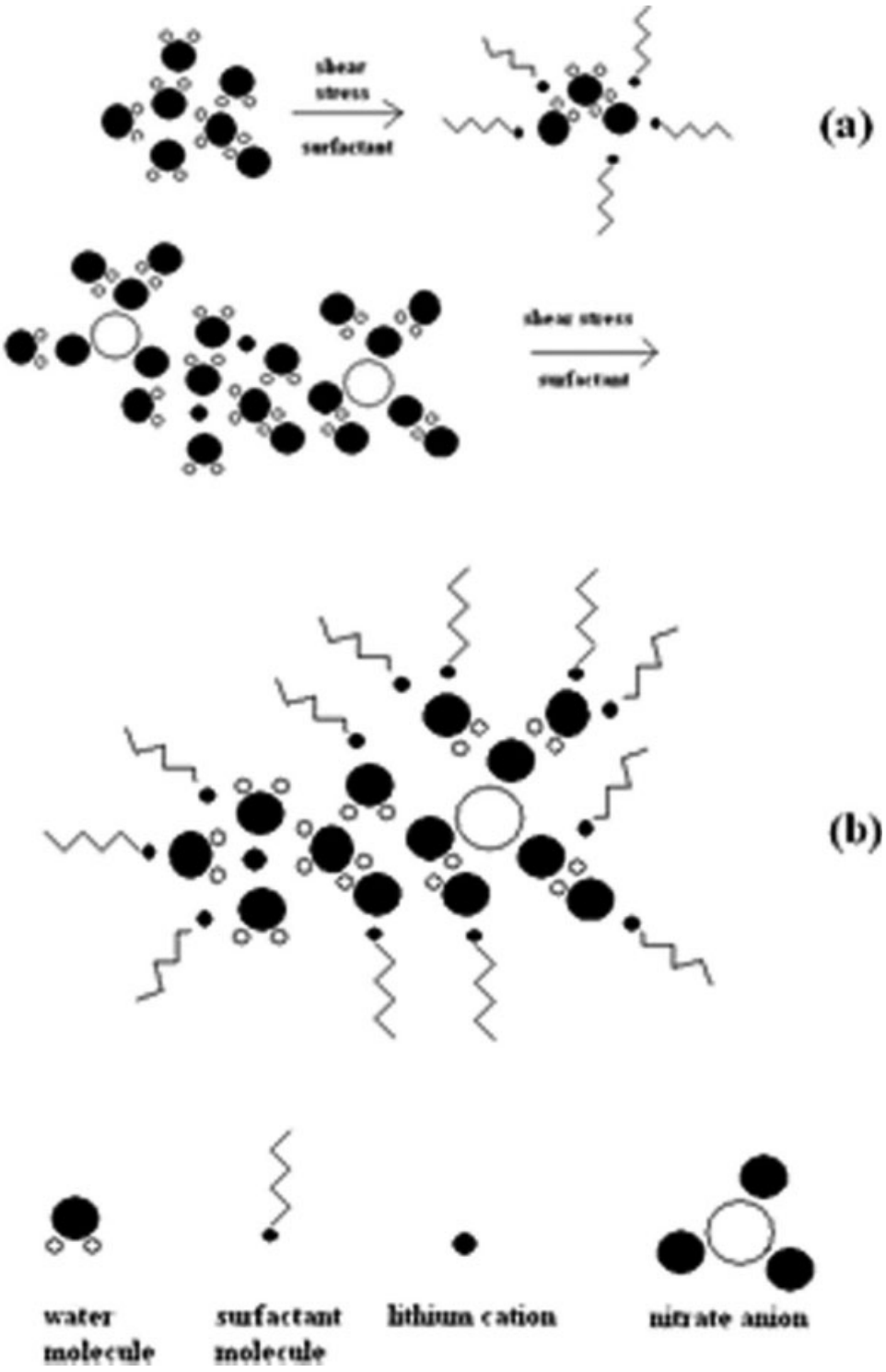

Figure 5. The effect of the presence of ions on the size of droplets under similar mechanical energy input intensity and surfactant concentration (for sake of simplicity, only lithium nitrate molecules have been shown): (a) in the absence of ions; (b) in the presence of ions.

for constant mechanical mixing intensity will increase, as observed experimentally.

To attenuate the solvation effect discussed earlier, use of ultrasound seems to be an effective solution. Figure 6 shows the effect of ultrasound treatment as a function of treatment time on the droplets size distribution in the absence of any additional mechanical mixing. It is observed that ultrasound treatment may result in slightly smaller droplets (42 nm instead of 50 nm) with respect to mechanical mixing albeit without droplets larger than 100 nm. Figure 6 shows that

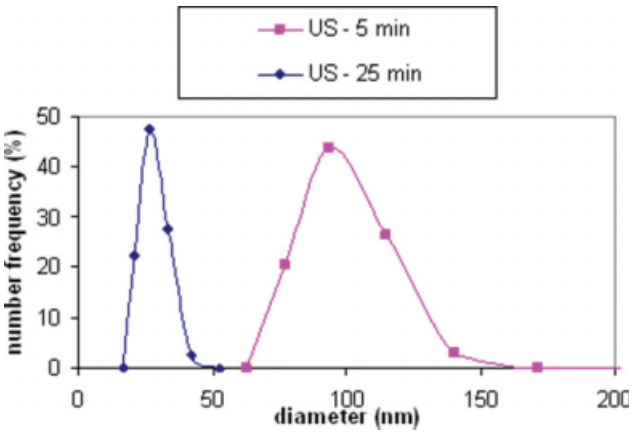

Figure 6. Droplets size distribution as a function of ultrasound treatment time.

[Color figure can be viewed in the online issue, which is available at www.interscience.wiley.com.]

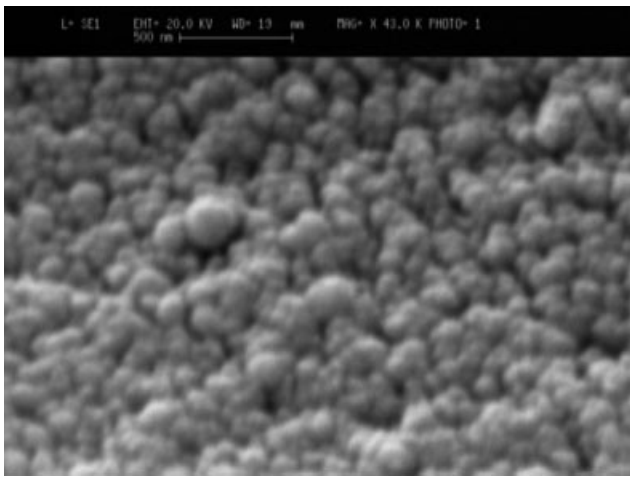

Figure 7. SEM picture of the surface of the α-Al_2O_3 plates film-coated with mixture C produced through mechanical mixing (1500 rpm, 25 min) after drying at 70°C for 1.5 h.

ultrasound treatment needs a minimum time period for being effective, clearly larger than 10 min. Moreover, employment of US treatment results in a mono-modal curve.

From an industrial point of view, it is important that droplets smaller than 100 nm (50 nm) using sole mechanical energy could be obtained. Certainly, use of more sophisticated impeller configurations that may impart increased shear stress at constant power input might reduce further the average size of the droplets and make it closer to the results obtainable using ultrasound technology which is more expensive.

We did not study the stability of the nanoemulsions at this stage. Micelle stability is an important factor in the production of W/O nanoemulsions. It is well known that the stability of nanoemulsions is mainly of a kinetic character.[16] As stated by Gutierrez et al.,[17] applications of nanoemulsions are strongly restricted by their stability, except for nanoparticle formation where the subsequent process of physical or chemical modification takes place within the period of stability of the nanoemulsions. In our case, the emulsions were stable enough to perform successfully the subsequent coating step through infiltration.

Figure 7 shows the surface of the film-coated α-Al_2O_3 porous support with mixture C produced through US treatment for 25 min after drying at 70°C for 1 h. The existence of nanosize entities is clearly observed. It should be emphasized that the aforementioned solid particles do contain lithium and magnesium salts, water, surfactant, cosurfactant and trace other organic materials. Figure 8 shows the STA diagrams of the cited sample. The two main weight losses occurring in the temperature ranges 300–500°C and 500–600°C are attributed to the decomposition of the magnesium and lithium salts, respectively. It is most probable that organic molecules leave the sample before 400°C. The exothermic double peak observed in the temperature range of 500–600°C is abnormal if attributed solely to the decomposition of magnesium nitrate. The authors of this study postulate that Li^+ cations diffuse into the magnesium nitrate molecules and substitute the Mg^{2+} cations due to the nearly similar size of the Li^+ and Mg^{2+} ions, especially at temperatures higher than 500°C. Such a substitution results in the weakening of the nitrate bonds (lithium-nitrate bonds with respect to magnesium-nitrate bonds) and eventually the partial decomposition at a temperature smaller than that of pure magnesium nitrate. The latter phenomenon is highly appreciated, as the final catalyst will assume a more intimate neighborhood of lithium and magnesium cations. This is of extreme interest for OCM catalysts. In addition, such a substitution inhibits to some extent escape of lithium through vaporization. This is desired, especially from a manufacturing point of view.

For producing nanocatalyst particles or catalyst coatings of thickness in the nanorange on porous support surfaces, one cannot rely solely on the successful coating of the aforementioned nanosize droplets (generally multilayers of such entities) on the internal surface of porous α-Al_2O_3 supports. Although Figure 7 gives a promising view for such a process, the thermal treatment of the dried coating is a crucial point for succeeding in obtaining the desired result. The following investigation reveals the optimal thermal treatment procedure needed to produce nano-$2Li_2O$/MgO catalyst particles on α-Al_2O_3 supports.

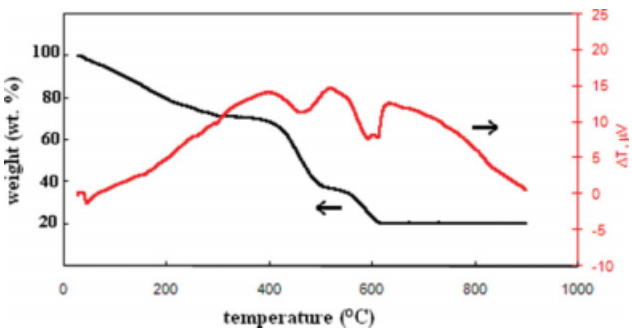

Figure 8. STA results of the coated support.

[Color figure can be viewed in the online issue, which is available at www.interscience.wiley.com.]

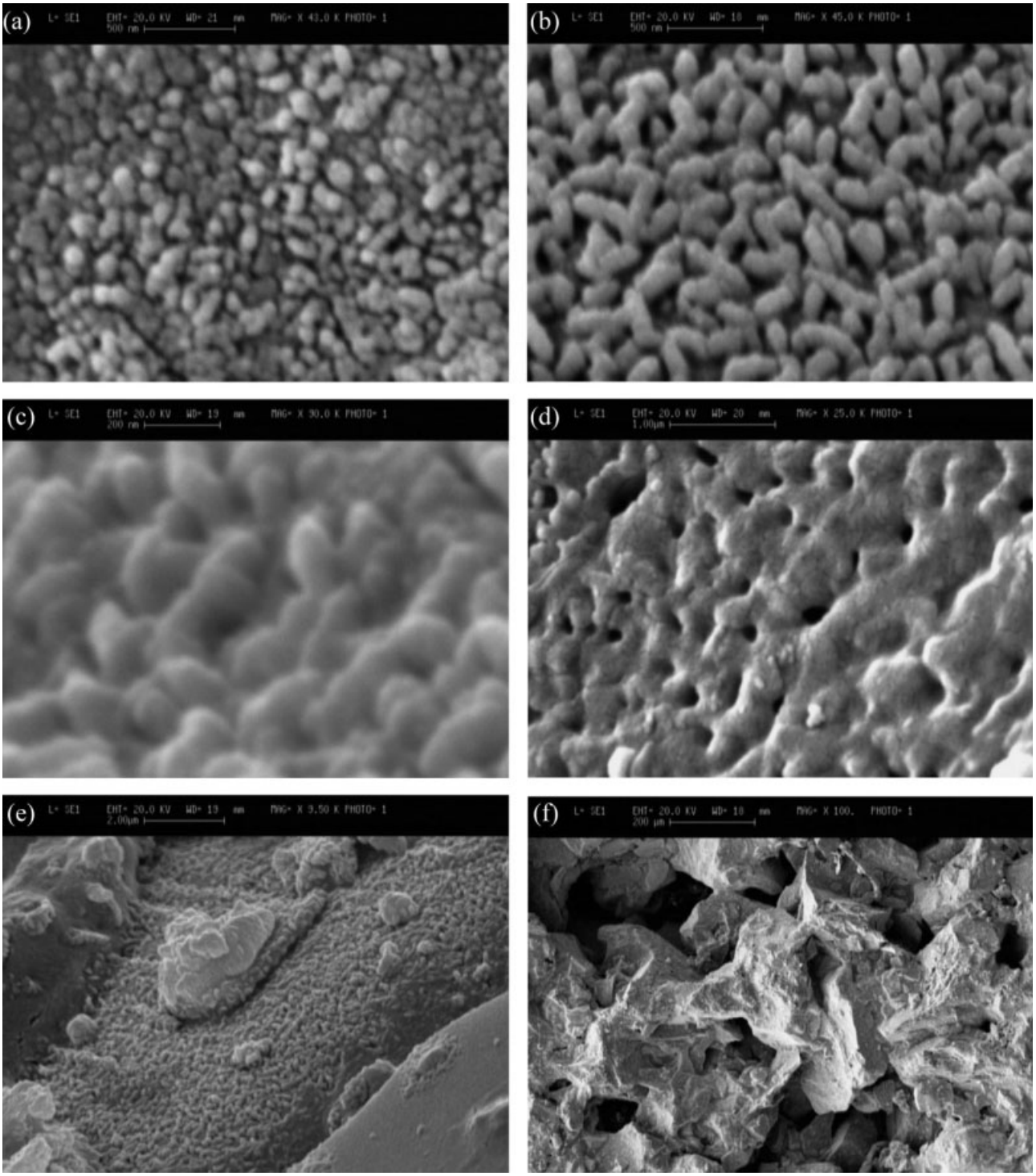

Figure 9. (a) Catalyst layer on support after thermal treatment at 250°C; (b) catalyst layer on support after thermal treatment at 900°C; (c) catalyst layer on support after thermal treatment at 1000°C; (d) catalyst layer on support after thermal treatment at 1250°C; (e) picture of the catalyst layer on support after thermal treatment at 900°C with low magnification to show partly the support; (f) picture of the support.

The coated and dried supports were subjected to 1.5 h thermal treatment at 250, 900, 1000, and 1250°C, respectively. The results are shown in Figures 9a–f. At a calcination temperature of 250°C, the nanoentities seem to detach as a result of partial shrinking. The latter particles still contain nitrate and organic impurities. At 900°C, isolated rod-like structures with a diameter smaller ca. 100 nm have grown on the surface. Increasing the calcination temperature to 1000°C, it is observed that the initial ''rod-like'' structures tend to spread on the support surface and attach to each

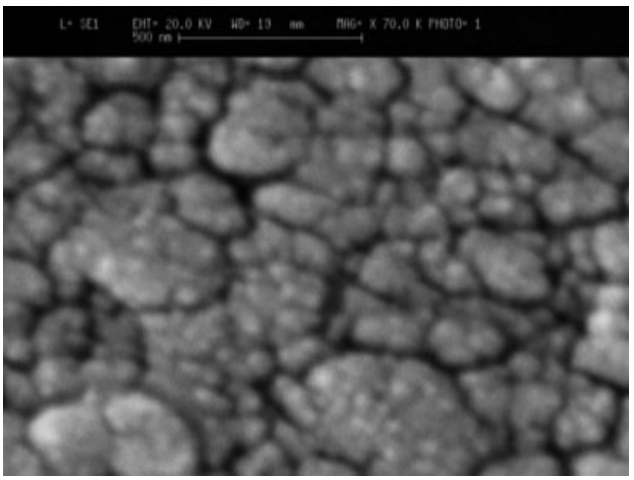

Figure 10. SEM picture of the surface of the α-Al_2O_3 plates film-coated with mixture C produced through mechanical mixing (1500 rpm, 25 min) after drying at 70°C for 1.5 h and thermal treatment at 900°C for 1.5 h.

other as a result of activated surface diffusion. Increasing further the calcination temperature to 1250°C, results in unwanted agglomeration. In addition, local growth of the thickness of the solid coating plus eventual production of "bare" surfaces on the support is observed. The latter exhibit themselves as "holes" on the surface (Figure 9d). Figure 9e shows a section of the catalyst/support and Figure 9f shows mainly the microstructure of the porous support used in this study.

Thus, it goes without saying that the US treatment results in much finer nanostructures after the thermal treatment process. Figure 10 shows an SEM picture of the catalyst particles obtained using mechanical mixing (1500 rpm, 25 min) after drying and thermal treatment at 900°C for 1.5 h. Compared to Figure 9b, it is observed that the sintered catalyst particles show a completely different morphology. Although the existence of entities smaller than 100 nm is evident, large agglomerates (>250 nm) are prevailing. No "rod-like" individual particles are observable. As explained previously, the pure mechanical mixing method (1500 rpm) produces ca. 50 nm droplets, but droplets larger than 100 nm still persist and consist 11% of the total droplets number. Larger sintered agglomerates due to these larger initial droplets may somehow inhibit the formation of the detached rod-shaped entities at higher temperatures by "swallowing" the smaller particles as a result of surface area minimization during calcination (sintering). The latter is not a complete explanation, as the sintered product still contains here and there entities smaller than 100 nm that do not have a "rod-like" morphology. In other words, we suspect that the molecular structure of the droplet/oil interface of the droplets produced by US treatment might be different to those produced by severe mechanical mixing. This is an open question worth further investigation. The BET-specific surface area measurements are summarized in Table 2. It is clearly observed that an abrupt increase of the specific surface area is observed for the US treated samples. This reconfirms the aforementioned discussion on the production of high-surface area nanorods on the surface due to the US treatment followed by thermal treatment.

Table 2. Specific Surface Area of Thermally Treated Samples (750°C, 1.5 h) and the α-Al_2O_3 Support

Sample	Mixing Intensity (rpm)	US Treatment (25 min)	BET Specific Surface ($m^2\ g^{-1}$)
α-Al_2O_3 Support	–	–	0.10
Coated and dried α-Al_2O_3 Support	500	No	0.41
Coated and dried α-Al_2O_3 Support	900	No	0.91
Coated and dried α-Al_2O_3 Support	1500	No	0.92
Coated and dried α-Al_2O_3 Support	–	Yes	6.08

An important point is the chemical analysis of the lithium and magnesium oxides of the nanoentities residing on the support internal surface. ICP analysis of the catalyst/support composite showed that that mass ratio Li/Mg is 1.14. This is accordance with the initial molar ratio of oxides Li_2O/MgO equal to 2 which is equivalent to a mass ratio of Li/Mg equal to 1.15. Actually we observed that using other concentrations of the initial solution A (see experimental section) retaining a fixed molar ratio of $LiNO_3/Mg(NO_3)_2$ of 4, the ICP analysis of the final catalyst/support composite always retained its mass ratio Li/Mg ca. 1.14. We were not able to identify the phase analysis of the nanoentities by XRD technique as the content of the nanocatalyst in the catalyst/support composite was ca. 0.48 wt %. A very small extra peak is observed for the nanocatalyst/support composite which we attribute to the catalyst particles but we cannot identify it according to existing databases (see Figure 11).

OCM reaction catalytic tests

A series of preliminary cross-flow experiments were performed to evaluate the effect of average reaction temperature on CH_4 conversion and product selectivity and yield. A CH_4/Ar mixture (35 mol % CH_4, flow rate = 500 $cm^3\ min^{-1}$) was introduced in the tube side of the reacting

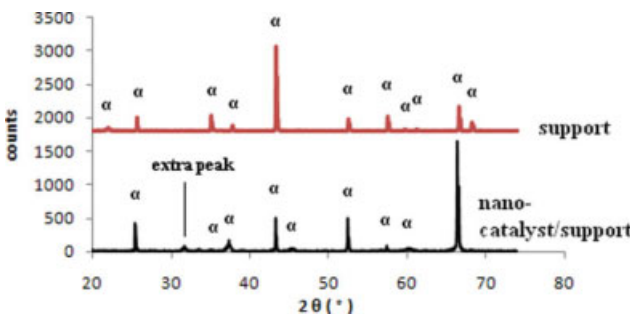

Figure 11. XRD pattern of the support (not ground) and nanocatalyst/support (ground) composite.

The preferred orientation of the support due to the existence of fused alumina particles is lost upon grinding in the case of the nanocatalyst/support. [Color figure can be viewed in the online issue, which is available at www.interscience.wiley.com.]

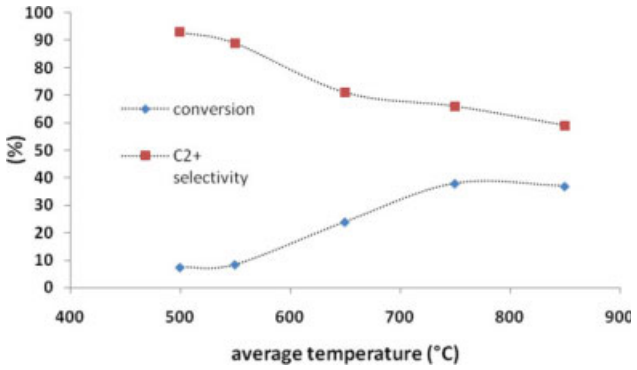

Figure 12. Variation of conversion and C_2^+ products selectivity as a function of reactor average temperature.

[Color figure can be viewed in the online issue, which is available at www.interscience.wiley.com.]

system and an O_2/Ar mixture (20 mol % O_2, flow rate = 550 cm^3 min^{-1}) was introduced in the shell side. The effect of average reaction temperature on the conversion of CH_4 is shown in Figure 12. It is observed that CH_4 conversion follows an increasing trend in the temperature range of 550–750°C. A maximum in conversion level (38%) is observed near 750°C. The same Figure shows the effect of reaction temperature on the selectivity of C_2^+ products. It should be mentioned that we did observe only C_2H_6 and C_2H_4 hydrocarbon products in the exiting stream. It is observed that selectivity follows a continuous decreasing trend throughout the whole temperature range understudy with an attenuated rate after 600°C. Figure 13 shows the variation of the yield of C_2^+ products vs. temperature. The trend resembles that of CH_4 conversion, with a maximum of 25% at 750°C.

The existence of a maximum in the yield of C_2^+ products as a function of temperature is a well known phenomenon. The latter is attributed to the two competing reactions of (a) gas-phase radicals transformation into hydrocarbons at lower temperatures and (b) gas-phase radicals reaction with oxygen resulting in oxygenate products at higher temperatures.

We did perform extra runs (blank runs) with the same gas feed streams flow rate and concentrations in the temperature

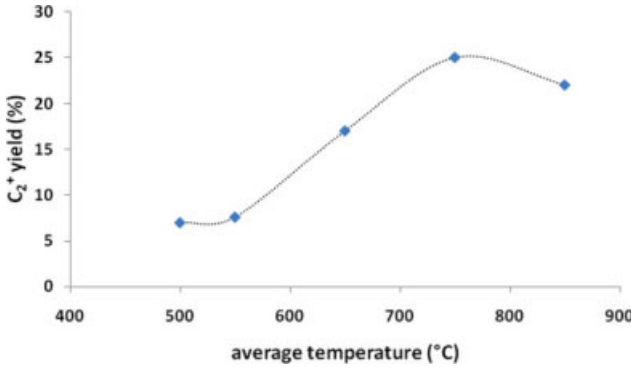

Figure 13. Variation of C_2^+ products yield as a function of reactor average temperature.

[Color figure can be viewed in the online issue, which is available at www.interscience.wiley.com.]

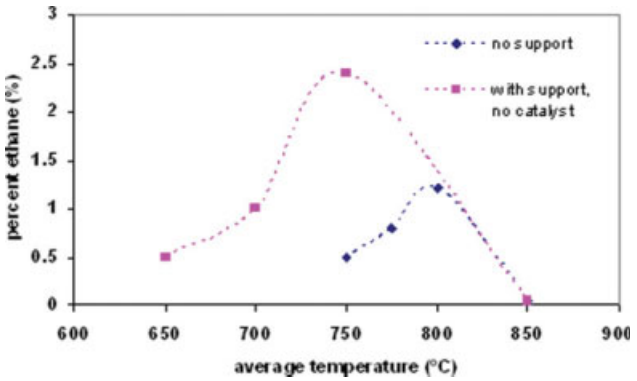

Figure 14. Variation of percent ethane (in the mixture of ethane +methane in the outlet stream) as a function of reactor average temperature for the sole support and no support cases (blank runs).

[Color figure can be viewed in the online issue, which is available at www.interscience.wiley.com.]

range of 650–850°C using the feed gas concentrations and flow rates used in the upper paragraph. These experiments were performed using a) a support without nanocatalyst rods and b) the reactor system itself in the absence of the catalyst/support body. The results are shown in Figure 14. A maximum in the percent of ethane is observed at 750 and 800°C for the sole support and no support cases, respectively. The yield of ethane is relatively low in both cases, especially at 750°C, and permits us to attribute the effect of different factors (like temperature, etc) on the observed kinetics in the case of the complete system to the presence of the catalyst nanorods within the support.

We chose 750°C as an optimum reaction temperature and studied the effect of feed streams flow rate on the reaction system for a constant CH_4/O_2 molar ratio of 1.6 and constant CH_4 and O_2 dilution in Ar of 35 and 20 mol %, respectively. The results for the CH_4/Ar mixture flow rates of 200, 500, and 700 cm^3 min^{-1} are shown in Figures 15 and 16. Conversion decreases less than 7% with increasing flow rate from

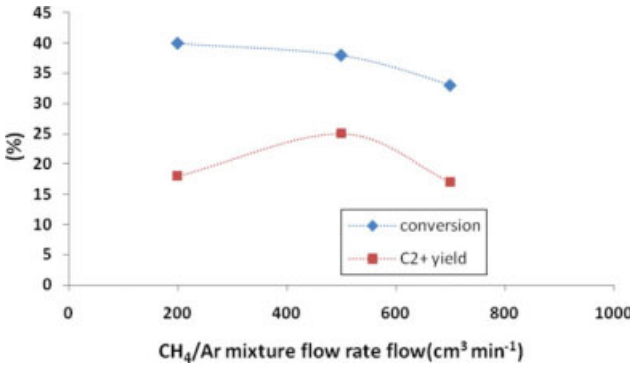

Figure 15. Variation of conversion and C_2^+ products yield as a function of the flow rate of the CH_4/Ar gas mixture at an average temperature of 750°C.

[Color figure can be viewed in the online issue, which is available at www.interscience.wiley.com.]

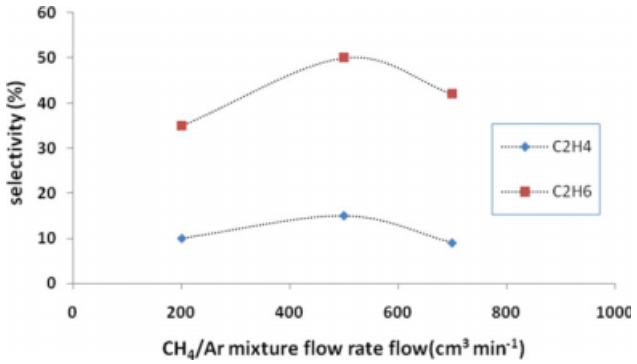

Figure 16. Variation of C_2H_4 and C_2H_6 products selectivity as a function of the flow rate of the CH_4/Ar gas mixture.

[Color figure can be viewed in the online issue, which is available at www.interscience.wiley.com.]

220 to 700 cm^3 min^{-1}. The selectivity of C_2H_6 and C_2H_4 products has a maximum at the flow rate of 500 cm^3 min^{-1}. The yield of C_2^+ products (Figure 15) also shows a maximum at a CH_4/Ar mixture flow rate of 500 cm^3 min^{-1}.

Increasing the flow rate of the feed gas streams decreases the residence time in the reactor system. Consequently, a continuous decrease in the conversion of CH_4 is expected. However, increasing the gas flow rates increases the turbulence within the void channels of the support and enhances the effective interaction of reactants with the surface catalyst nanorods. The latter phenomenon increases the selectivity vs. C_2^+ products. As a result of these two phenomena, a maximum of 25% in the yield of C_2^+ products is observed at a flow rate of 500 cm^3 min^{-1}.

The dilution extent of the CH_4 and O_2 gas streams also affects the reaction kinetics. For a constant average reaction temperature of 750°C and constant CH_4/O_2 molar ratio of 1.6, the dilution of CH_4 was varied in the range of 10 to 50 vol %. The total gas flow rate was 1050 cm^3 min^{-1} in all the experiments. The results are shown in Figure 17. It is observed that, as far as the yield of C_2^+ products is concerned, there exists an optimum inert gas concentration for

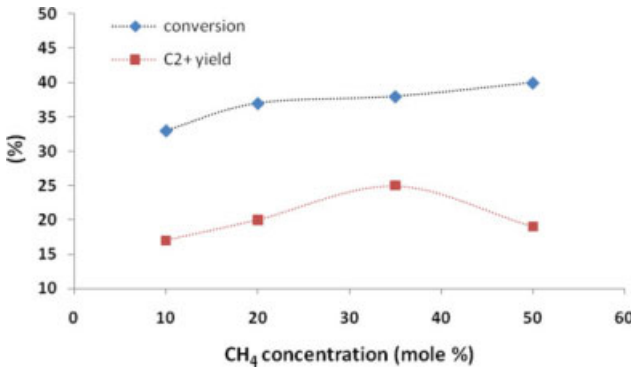

Figure 17. Methane conversion and C_2^+ yield as a function of methane concentration in the feed stream.

[Color figure can be viewed in the online issue, which is available at www.interscience.wiley.com.]

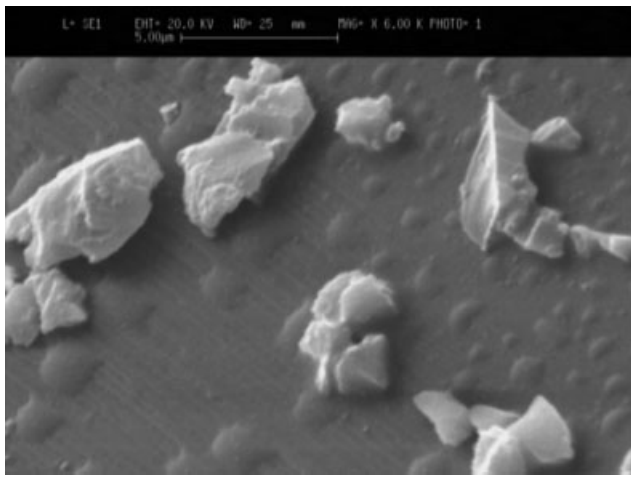

Figure 18. SEM picture of the "conventional" catalyst/support composite.

the CH_4/Ar stream resulting in a maximum yield of 25%. The latter phenomenon is attributed to the presence of gas phase radicals (like methyl radicals) as intermediate species. It has been reported that inert gases may "stabilize" radicals leading in higher yields of C_2^+ products.[18]

Up to this point, the optimum C_2^+ products yield determined experimentally has been 25% (38% CH_4 conversion and C_2^+ products selectivity of 66%). This has been obtained for a cross flow configuration at an average reaction temperature of 750°C, CH_4/Ar mixture flow rate of 500 cm^3 min^{-1} with 35 mol % CH_4 and a O_2/Ar mixture flow rate of 550 cm^3 min^{-1} with 20 mol % O_2. Such a yield has been reported only for Rb_2WO_4/SiO_2 catalyst but at 850°C.[19] Our new nanocatalyst reaction system is able to produce this yield with a reaction temperature 100°C lower.

At this stage, it is imperative to elucidate if the high C_2^+ products yield is mainly due to a nanoeffect (nanosize of the catalyst particles) or other factors are involved. Figure 18 shows an SEM picture of the conventional catalyst. The average size of the particles lying on the support is larger than 1 μm. The content of the catalyst particles is ca. 0.96 wt %, about 100% more than the catalyst content of the nanocatalyst/support composite (0.48 wt %). The Li and Mg concentration of the aqueous solution containing the metal nitrates has been the same used for producing the nanocatalyst. The XRD diagram (not shown) showed the same extra peak at a 2θ angle of 31.5°. The specific surface area of the conventional catalyst/support composite was measured to be 0.33 m^2 g^{-1}. Using the optimal process conditions indicated previously for the nanocatalyst (cross flow configuration at an average reaction temperature of 750°C, CH_4/Ar mixture flow rate of 500 cm^3 min^{-1} with 35 mol % CH_4 and a O_2/Ar mixture flow rate of 550 cm^3 min^{-1} with 20 mol % O_2) the conventional one was subjected to 8 and 24 h duration catalytic performance tests. The results are summarized in Table 3. With respect to the nanocatalyst, the conventional one results in significant lower conversion and selectivity. This is while the conventional catalyst composite contains ca. 100 wt % more catalyst particles. A 40% reduction in the selectivity is observed for the conventional composite.

This means that the activity and yield for the conventional catalyst/support composite is substantially lower with respect to the nanocatalyst/support composite. Up to this point it is quite clear that the size of the catalyst might be a determining factor in obtaining the high yield of the C_2^+ products. Nonetheless, the latter phenomenon might be due to the specific reactor configuration used in this study, i.e., cross-flow configuration.

To study the role of the hydrodynamic configuration of the system on the reaction yield, we performed a catalytic run using the nanocatalyst/support composite under the following process conditions: Uniaxial flow configuration, average reaction temperature of 750°C, $CH_4/O_2/Ar$ mixture flow rate of 1050 cm^3 min^{-1} (16.68 mol % CH_4, 10.47 mol % O_2 and 72.85 mol % Ar). Actually, all the reactant and inert gas flows of the cross-flow system with the optimal conditions were introduced into the tube side. The results were as follows: CH_4 conversion 41%, C_2H_6 selectivity 52% and C_2H_4 selectivity 10%. Correspondingly, the yield of C_2H_6, C_2H_4 and C_2^+ was calculated as 21, 4, and 26 %, respectively. Compared with the results due to the cross-flow system for the optimal conditions (yield of C_2H_6, C_2H_4, and C_2^+ equal to 19, 8, and 25%, respectively), it is observed that the overall yield of C_2^+ products is approximately unchanged. This outcome shows that the hydrodynamic configuration of the system is not a major factor resulting in the high yield of the C_2^+ products.

Based on the previous discussion, it may be stated that the high yields of C_2^+ products obtained is mainly due to a nanoeffect. The cross-flow configuration increases the yield of C_2H_4 ca. 100% while the total yield of the C_2^+ products is rather unchanged.

Table 3 comprehends also some information on the deactivation tendency of the catalyst/support composite. It is observed that the nanocatalyst/support composite undergoes some 8.0% decrease in yield after 24 h. This is while the conventional catalyst/support undergoes a substantial decrease of 33.3%. Catalyst deactivation may mainly be due to coking and sintering (agglomeration and loss of surface area) effects. Our results show that the nanocatalyst is significantly more robust and stable against such deactivation processes. Figure 19 shows a section of the nanocatalyst after 24 h on test. It is observed that the morphology of the nanorods is saved to a great extent. BET measurements also showed that the nanocatalyst/support composite underwent a 4% decrease in surface area while the conventional catalyst/support composite suffered from a 12% decrease in surface area.

Table 3. Results of the Catalytic Tests for the Nano and Conventional Catalyst/Support Composites as a Function of Run Time for the Optimum Process Conditions*

Catalyst/Support Type	Catalytic Test Duration (h)	CH_4 Conversion (%)	C_2^+ Selectivity (%)	C_2^+ Yield (%)
Conventional	8	19	40	7.5
Conventional	24	15	34	5
Nanocatalyst	8	38	66	25
Nanocatalyst	24	36	63	23

*The optimum process conditions are as follows: cross flow configuration at an average reaction temperature of 750°C, CH_4/Ar mixture flow rate of 500 cm^3 min^{-1} with 35 mol % CH_4 and a O_2/Ar mixture flow rate of 550 cm^3 min^{-1} with 20 mol % O_2.

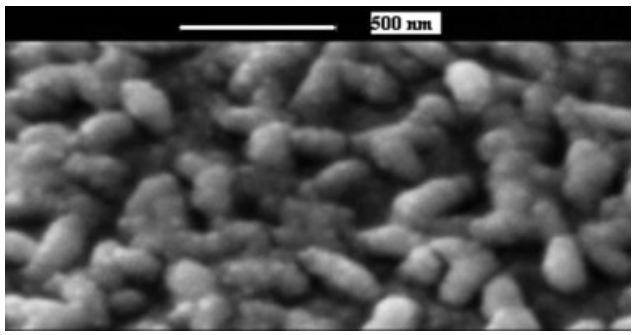

Figure 19. SEM picture of the nanocatalyst after 24 h on test.

Conclusions

A novel and simple technique for the production of rod-shaped $2Li_2O/MgO$ nanoparticles on the internal surface of α-Al_2O_3 supports has been disclosed. The method is based on nanoemulsion production (W/O system), coating the nanodroplets on support by infiltration and subsequent calcination by applying proper thermal treatment. The peculiarity of our preparatory recipe is the success in producing ''detached'' nanosized entities on the support surface.

It should be emphasized that, theoretically, the initial droplets should not absolutely be of a size smaller than 100 nm. Recall that the droplets contain a large volume percentage of water molecules which egress the system upon drying and high-temperature thermal treatments. Instead, the interaction between the coated neighbor droplets during heat treatments, especially during drying, is of extreme importance. Material should not cross over the droplets boundaries during the latter process, so that droplet shrinking and detachment occurs upon egress of water molecules and gaseous decomposition products of organic material and metal nitrates.

We speculate that the nature of droplets, or at least the droplet/oil interface molecular structure, of a size smaller than 100 nm is not identical for the US and mechanical mixing methods. This is matter of debate and subject of our future studies.

The catalytic performance of the new nanocatalyst/alpha alumina support system for the OCM reaction has been investigated in a specially designed cross flow configuration for the reactor system. The results are promising: A yield of C_2^+ products equal to 25% may be obtained at an average temperature of 750°C. Preliminary experiments show that the gradual introduction of O_2 from the lateral porous walls of the reacting system favors the production of ethylene.

It was shown that the enhanced catalytic properties of the new catalyst/support composite may be attributed to nanoeffects. The novel nanocatalyst/support composite has substantially better catalytic and stability with respect to conventional catalyst/support composites.

Acknowledgments

The authors gratefully acknowledge the financial support by the Petrochemical Research and Technology Co. under the contract No. 84111202.

Literature Cited

1. Johnson MA, Stefanovich EV, Truong TN. An ab initio study on the oxidative coupling of methane over a lithium doped MgO catalyst, surface defects and mechanism. *J Phys Chem B*. 1997;101:3196–3201.
2. Lafarga D, Santamaria J, Menendez M. Methane oxidative coupling using porous ceramic membrane reactors-I. Reactor development. *Chem Eng Sci*. 1994;49:2005–2013.
3. Coronas J, Menendez M, Santamaria J. Methane oxidative coupling using porous ceramic membrane reactors-II. Reaction studies. *Chem Eng Sci*. 1994;49:2015–2025.
4. Lee Y, Lee J, Jin Bae C, Park J-G, Noh H-J, Park J-H, Hyeon T. Large-scale synthesis of uniform and crystalline magnetite nano-particles using reverse micelles as nano-reactors under reflux conditions. *Adv Func Mater*. 2005;15:503–509.
5. Li GL, Wang GH. Synthesis of nano-meter-sized TiO2 particles by a micro-emulsion method. *Nano Struc Mater*. 1999;11:663–668.
6. Porras M, Martinez A, Solans C, Gonzales C, Gutierrez JM. Ceramic particles obtained using W/O nano-emulsions as reaction media. *Colloid Surf Physicochem Eng Aspect*. 2005;270–271:189–194.
7. Elm Svensson E, Nassos S, Boutonnet M, Jaeras SG. Micro-emulsion synthesis of MgO-supported LaMnO3 for catalytic combustion of methane. *Catal Today*. 2006;117:484–490.
8. Porras M, Solans C, Gonzales C, Gutierrez JM. Properties of water-in-oil (W/O) nano-emulsions prepared by a low-energy emulsification method. *Colloid Surf Physicochem Eng Aspect*. 2008;324:181–188.
9. He Y, Yang B. Cheng G. On the oxidative coupling of methane with carbon dioxide over CeO2/ZnO nano-catalysts *Catal Today*. 2004;18:595–600.
10. Wang XG, Kawanami H, Dapurkar SE, Venkataramanan NS, Chatterjee M, Yokoyama T, Ikushima Y. Selective oxidation of alcohols to aldehydes and ketones over TiO2-supported gold nanoparticles in supercritical carbon dioxide with molecular oxygen. *Appl Catal A Gen*. 2008;1–2:86–90.
11. Yamashita H, Miura Y, Mori K, Ohmichi T, Sakata M, Mori H. Synthesize of nano-sized Pd metal catalyst on Ti-containing zeolite using a photo-assisted deposition (PAD) method. *Catal Lett*. 2007;114:75–78.
12. Lafarga D, Santamaria J, Menendez M. Methane oxidative coupling using porous ceramic membrane reactors-I-Reactor development. *Chem Eng Sci*. 1994;49:2005–2013.
13. Holmberg K. *Handbook of Applied Surface and Colloid Chemistry*. West Sussex: Wiley, 2002.
14. Beduneau A, Saulnier P, Anton N, Hindre F, Passirani C, Rajerison H, Noiret N, Benoit GP. Pegylated nano-capsules produced by an organic solvent-free method: evaluation of their stealth properties. *Pharm Res*. 2006;23:2190–2199.
15. O'M Bokris J, Reddy AKN. *Modern Electrochemistry*, 2nd ed. New York: Plenum/Rosetta, 1976.
16. Solans C, Esquena J, Forgiarini AM, Uson N, Morales D, Izquierdo P, Azemar N, Garcia-Celma MJ. Nano-emulsions: formation, properties and applications. *Surf Sci Ser*. 2003;109:525.
17. Gutierrez JM, Gonzales C, Maestro A, Sole I, Pey CM, Nolla J. Nano-emulsions: new applications and optimization of their preparation. *Curr Opin Coll Int Sci*. 2008;13:245–251.
18. Sinev MY, Tulenin YP, Kalashnikova OV, Bychkov VY, Korchak VN. Oxidation of methane in a wide range of pressures and effect of inert gases. *Catal Today*. 1996;32:157–162.
19. Holmen A. Direct conversion of methane to fuels and chemicals. *Catal Today*. 2009;142:2–8

Manuscript received Apr. 18, 2009, revision received June 23, 2009, and final revision received June 25, 2009.